Embeddable wireless strain sensor based on resonant rf cavities

J. Chuang, D. J. Thomson, and G. E. Bridges
Electrical and Computer Engineering, University of Manitoba, 15 Gillson Street, Winnipeg, Manitoba R3T 5V6, Canada

(Received 31 October 2003; accepted 22 July 2005; published online 20 September 2005)

In this article we describe a type of sensor to monitor strain. The strain sensor is a passive device that can be embedded or attached to a structure and then remotely interrogated though a wireless interface. Such a system has the advantage of requiring no permanent physical connection, either electrical or optical, to an interrogation system. The sensor is a conducting coaxial electromagnetic cavity that is embedded in or bonded to the structure in which strain is to be measured. The cavity will exhibit resonance for electrical wavelengths two times the cavity length. Changes in the structure's dimensions will be reflected in changes in the dimensions of the cavity, and will result in a shift of the resonant frequency of the cavity. The sensor incorporates an antenna so that the resonant frequency of the cavity can be determined by remote interrogation. The acquired resonant frequency is then used to calculate the strain in the structure. The sensor presented in this article operates at a frequency of approximately 2.45 GHz, and exhibits a shift in resonance of 2.45 kHz per microstrain ($\mu\varepsilon$). We have demonstrated a strain sensitivity of less than 1 $\mu\varepsilon$ with a bandwidth of 25 Hz. This class of embeddable sensor is expected to have the greatest application in monitoring the health of, and assessing damage in, civil structures. © *2005 American Institute of Physics.* [DOI: 10.1063/1.2051808]

I. INTRODUCTION

Structural health monitoring is expected to move from demonstration projects into engineering practice over the next few years. The availability of sensors that are well matched to the needs of structural health monitoring will be key to successfully making this move.[1] Ideally a strain sensor should offer an unambiguous measurement of strain with high resolution. It should be durable with a life span comparable to that of the structure, and make use of widely available technology. A number of sensing technologies have been developed with this need in mind. Fiber-optic-based sensors have received considerable attention since they are very compact and can have very high resolution.[2–4] However, they have inherent problems such as fragility and susceptibility to damage during installation.[5,6] Another major drawback of fiber-optic sensors is that they, like traditional metal foil strain gauge sensors, still require a physical connection between sensor and the interrogation unit that collects, analyzes, and stores data from the sensor. This connection is susceptible to weathering, corrosion, and fracture. In addition, the associated data acquisition electronics requires continuous power.

In this article we present a wireless sensor that makes use of widely available radio frequency (rf) technology to measure strain through changes in the resonant frequency of the sensor with applied strain. This strain sensor is a passive sensor that can be interrogated through an attached antenna and hence has the advantage of requiring no permanent electrical or optical connection to an interrogation system and no internal power supply. As rf signals can penetrate a significant depth into concrete,[7] it is possible to embed these sensors within a concrete structure or other material that has similar rf transmission properties. The sensor employed in this article is a metal cylinder with a coaxial cavity machined out of its center. We present the theoretical basis of the sensor, measurements of the electromagnetic characteristics of the sensor, measured changes in the sensor's resonant frequency with applied strain, preliminary signal-to-noise estimates, as well as initial results from remote interrogation of the sensor using a simple loop antenna.

II. PRINCIPLE OF OPERATION

A block diagram of the sensing system is illustrated in Fig. 1. The sensor is a one-port high-Q resonant network. It is interrogated by sending a rf signal and subsequently detecting the reflected signal when the cavity is near resonance. There are many ways to interrogate the resonant frequency of the sensor. In the method we have employed a pulse modulated rf signal is transmitted from the interrogation system to the embedded cavity, where it excites an electromagnetic field. The maximum field will be generated when the frequency of the incoming signal is at the cavity's loaded resonant frequency. Eventually the field in the cavity will reach equilibrium. In our system the cavity has a resonant frequency of approximately 2.45 GHz with an unloaded Q greater than 2000 so that equilibrium is reached in approximately 400 ns. After equilibrium is achieved, the input signal is switched off and the stored energy will reradiate out of the resonator. The interrogation unit then acts as a receiver, where the returned signal is an exponentially decaying rf signal. The signal is amplified and sent to a rf peak detector such that the returned signal power can be measured. To determine the resonant frequency of the cavity, and hence the

 © 2005 American Institute of Physics

Downloaded 30 Nov 2011 to 132.170.72.241. Redistribution subject to AIP license or copyright; see http://rsi.aip.org/about/rights_and_permissions

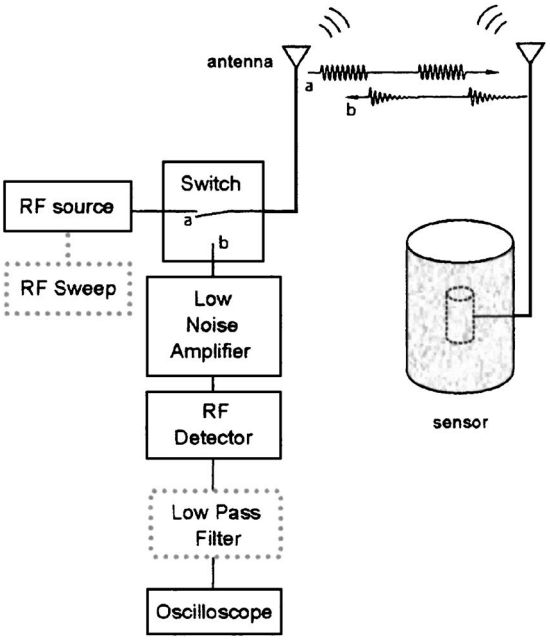

FIG. 1. Schematic of the sensor and interrogation system. A FM modulated signal is transmitted to the embedded sensor. The received signal is directed to a low noise amplifier and a rf detector, and then to an oscilloscope or lock in-amplifier, which is referenced to the FM modulation frequency.

applied strain, the transmitted rf signal is swept over a range of frequencies to find the frequency at which the power received at the detector is a maximum.

III. THEORETICAL BASIS OF SENSOR

A schematic diagram of the sensor is shown in Fig. 2. There are many types of electromagnetic cavities with resonant frequencies that change with dimension. The sensor we have employed is a simple coaxial cavity with length l. A small wire probe extends into the cavity to excite the electromagnetic field. The cavity can support many possible resonant modes, the dominant mode (and lowest resonant frequency) being the lowest TEM mode, where the field is a maximum at the center of the cavity and zero at the ends.[8] The TEM_{001} resonant frequency is

$$f_r = \frac{c}{2l\sqrt{\varepsilon_r}}, \tag{1}$$

where c is the speed of light in vacuum and ε_r is the relative permittivity of the material filling the coaxial cavity (in our case, air, $\varepsilon_r \sim 1$). When the structural material in which the sensor is encased is stressed, it will force a change in the dimensions of the cavity. The longitudinal dimensional change, Δl, will result in a shift in resonant frequency that can be used to unambiguously determine the strain, $\Delta l/l$, in the structure. If the elastic properties of the sensor material differ from the material in which it is embedded, a gauge factor may be required. For small strains, $\Delta l \ll l$, the shift in resonant frequency can be approximated as

$$f_{\text{strained}} = \frac{c}{2(l+\Delta l)} = \frac{c}{2l}\left(\frac{1}{1+\varepsilon}\right) \approx f_{\text{unstrained}}(1-\varepsilon), \tag{2}$$

$$\Delta f_r = f_{\text{strained}} - f_{\text{unstrained}} \approx -f_{\text{unstrained}}\varepsilon, \tag{3}$$

where $\varepsilon = \Delta l/l$ is the strain. Typically the structure is under compression resulting in a positive shift in frequency.

As long as the unstrained resonant frequency is known, then the strain can be determined with the same accuracy as the resonant frequency can be measured. One advantage of this approach is that rf signals can be generated with very high accuracy and stability. Radio frequency signal generating sources can be frequency locked to quartz crystal oscillators, which are easily obtained with errors of less than one part per million and stability within a few parts per billion.[9]

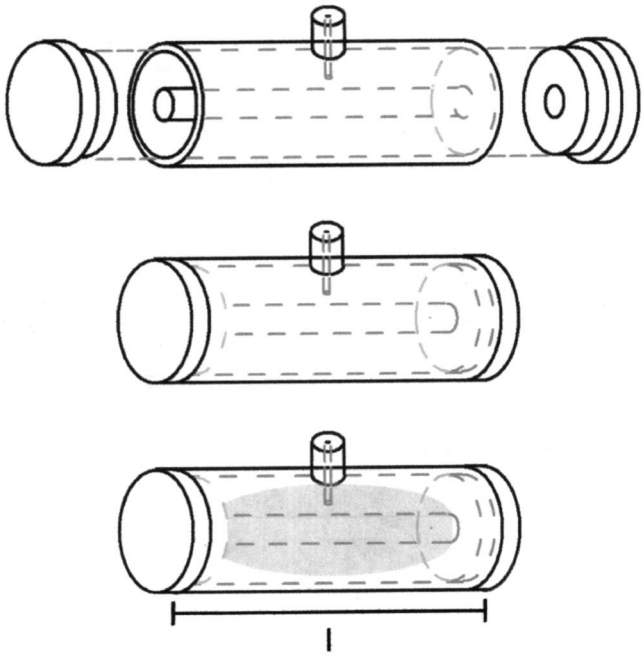

FIG. 2. Diagram of the electromagnetic coaxial cavity sensor. The ends are of press-fit construction. The dominant TEM_{001} resonant mode is shown in the bottom diagram.

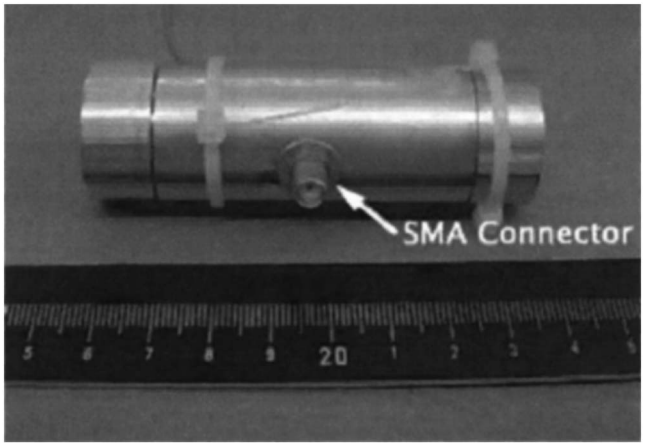

FIG. 3. Photograph of coaxial cavity sensor. This sensor is constructed from aluminum. The sensor used in this article is identical in dimension, but machined from brass.

IV. COAXIAL RF RESONANT STRAIN SENSOR

A photograph of a fabricated cylindrical cavity sensor is shown in Fig. 3. The sensor is machined out of brass or

Downloaded 30 Nov 2011 to 132.170.72.241. Redistribution subject to AIP license or copyright; see http://rsi.aip.org/about/rights_and_permissions

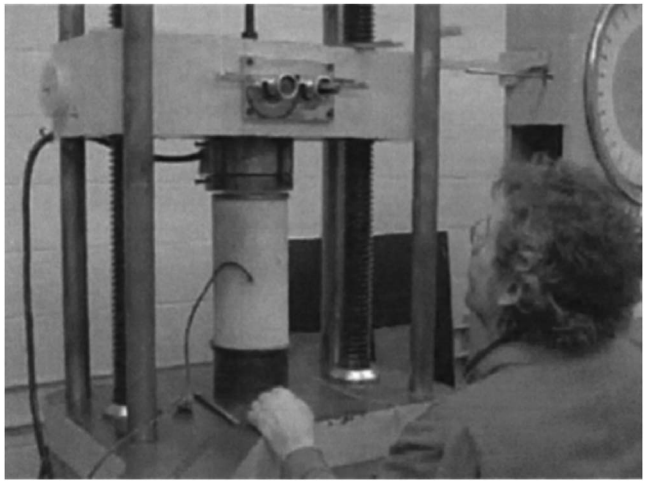

FIG. 4. Photograph of the concrete test cylinder with embedded sensor mounted in a load frame for compression testing.

aluminum with press-fit ends. The coaxial cavity is $l = 44.3$ mm long, resulting in an unstrained resonant frequency of approximately 2.45 GHz and an expected shift in resonant frequency of $\Delta f_r \cong 2.45\ \text{kHz}/\mu\varepsilon$. The rf signal is coupled to the sensor cavity through a 50-Ω SMA—type connector that has a wire probe center conductor that protrudes into the cavity.

For preliminary tests of the resonant cavity sensor, the sensor was encased in concrete while being directly connected to a network analyzer with a coaxial cable, enabling direct measurement of its input impedance characteristics (via the measured reflection coefficient). The sensor was prepared for encasement in concrete by sealing the seams and joints with a layer of nitrile rubber. The outside of the sensor was then wrapped in a thick layer of butyl rubber, which was stretched over the sides of the sensor and over the connector, leaving only the ends of the sensor exposed to the concrete. The prepared sensor was then embedded in the center of a concrete cylinder. A traditional metal foil strain gauge was applied to the outside of the concrete cylinder to provide a reference strain measurement. A load frame, as shown in Fig. 4, was used to apply a load to the concrete cylinder and strain the sensor. Measurements of strain and resonant frequency were obtained by cycling loads from 0 to 66 723 N, corresponding to approximately 0–170 microstrain.

The measured reflection coefficient, S_{11}, versus frequency for the cylindrical cavity resonator under no strain is shown in Fig. 5, indicating a resonant frequency of approximately 2.4215 GHz with a Q greater than 2000. Figure 6 shows measurements of the resonant frequency shift, Δf_r, versus applied strain (as measured using the metal foil strain gauge) during compression testing. The measured result shows a response of 2.6 kHz per $\mu\varepsilon$ with a high degree of linearity up to 130 $\mu\varepsilon$. Strain levels beyond 130 $\mu\varepsilon$ exhibited an uncharacteristic decrease in the resonant frequency shift. This behavior is due to the construction method used for this particular cavity, which employs press-fit ends. The ends may cause the cavity dimensions to change in an unpredictable manner due to frictional forces that are overcome near 53 000 N. This nonlinearity can be addressed by securing the ends more rigidly to the cylinder walls, such as by a welding process.[10]

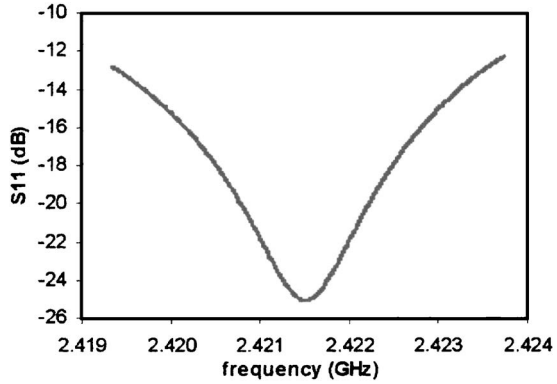

FIG. 5. Measured reflection coefficient for a brass cylindrical resonator embedded in concrete with zero applied load. The figure indicates a resonant frequency of 2.4215 with a Q greater than 2000.

V. ANTENNA FOR WIRELESS INTERROGATION

One of the key elements of the sensor system is the antenna that is attached to the cavity sensor. There are many types of antennas that could be used for this application. We have initially employed a loop antenna, as it is omnidirectional, has a fairly wide bandwidth, and a balun can be easily incorporated into its design. Ease of fabrication and integration, as well as life span and durability of the antenna when embedded in concrete, were also considered. Initial tests were conducted using a loop antenna with a $\lambda/2$ balun.[11] The antenna was constructed from copper tubing with 6-mm-diam and 0.79-mm-thick walls. The balun and feed cable were constructed from a 40-mm-long, 2.18-mm-outer-diam, semirigid copper coaxial cable with a dielectric constant of 2.3. A photograph of the antenna is shown in Fig. 7. The circumference of the loop was 170 mm (-1.4λ in air), selected to optimize the directivity and impedance match of the antenna, and the diameter was selected to minimize variability of the input impedance due to variations in the electrical properties of the medium surrounding the antenna when it is embedded in concrete.

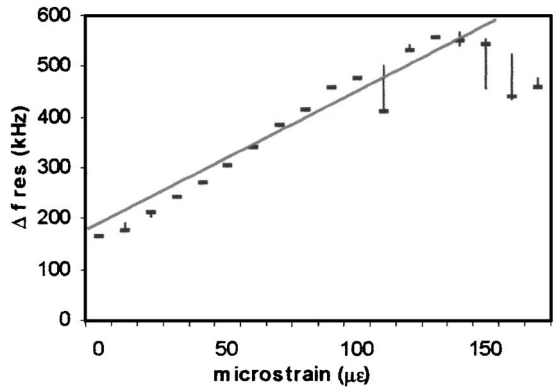

FIG. 6. Change in Δf_r as a function of applied strain to the concrete block, as measured by a traditional strain gauge, indicating linearity up to 130 $\mu\varepsilon$. The solid line shows the expected result of 2.42 kHz/$\mu\varepsilon$.

Downloaded 30 Nov 2011 to 132.170.72.241. Redistribution subject to AIP license or copyright; see http://rsi.aip.org/about/rights_and_permissions

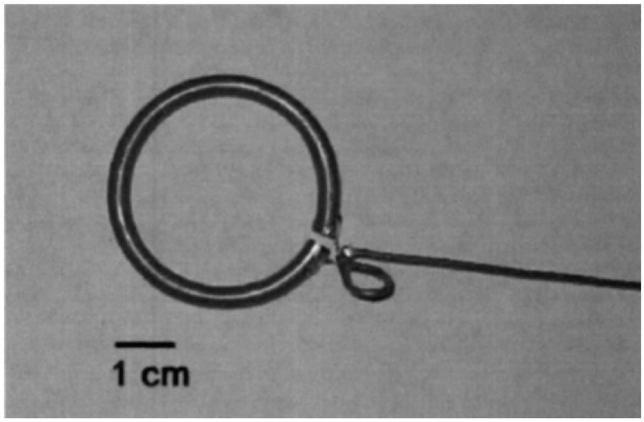

FIG. 7. Photograph of the loop antenna to be mounted with the sensor.

VI. INTERROGATION SYSTEM OPERATION

To test the response of the embedded sensor with the loop antenna by remote interrogation, the system illustrated in Fig. 8 was employed. A rf signal from a generator (Rohde & Schwarz SMT-03) is coupled to a 2.4-GHz patch antenna (Demarc Technologies Group SPLG11F) through an absorptive SPDT switch (Minicircuits ZASWA-2-50DR) and transmitted to the sensor. The received signal from the sensor is directed through the switch to a low noise amplifier (Minicircuits ZHL-1724MLN-SMA), a diode rf peak detector (Anritsu 73N50) and then to a lock-in amplifier (Stanford Research SR510). The function of the switch in the system is to separate the transmitted and received signals as well as to act as a time-domain gate for the received signal. By controlling the on–off timing during the received signal period, unwanted reflections from obstacles other than the sensor can be eliminated. For the results presented in this article, the switch was modulated at rate of 5 MHz. A photograph of the test setup is shown in Fig. 9, where the interrogation system antenna and sensor antenna are separated by approximately

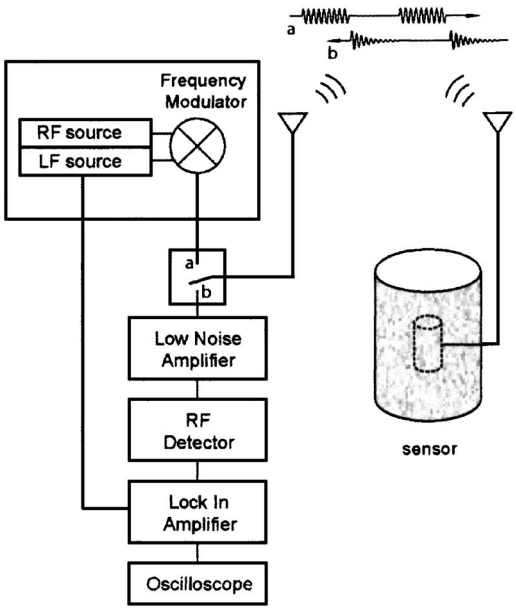

FIG. 8. Block diagram of a phase sensitive interrogation system.

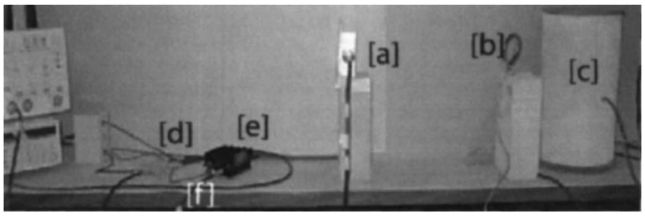

FIG. 9. Photograph of the setup to test wireless interrogation of the cavity/loop antenna sensor. Shown are (a) transmitter/receiver patch antenna, (b) loop antenna, (c) concrete cylinder with embedded sensor, (d) rf switch, (e) low-noise amplifier, and (f) rf detector.

50 cm. The signal loss for the wireless channel, as measured between the terminals of the two antennas using a network analyzer, was approximately −25 dB.

To minimize the effects of most types of noise, a phase-sensitive detection technique is employed in the interrogation system. The rf signal from the high-frequency signal generator is frequency modulated at a fairly low rate (f_m=15 kHz in our system) before being coupled to the antenna. This produces a 15-kHz signal at the output of the rf detector that is proportional to the frequency shift of the resonant peak (as described below). The lock-in amplifier, which is phase referenced to the low frequency modulation signal at f_m, then produces a phase-sensitive signal that is proportional to the shift in resonant frequency and hence the strain. The location of the resonant frequency can be determined by sweeping the rf center frequency and monitoring the lock-in output signal.

The operation of the phase-sensitive detection scheme is explained by considering a typical frequency response of the detector versus rf frequency, $V(f)$, as depicted in Fig. 10. The shape of the response will be dictated primarily by the fre-

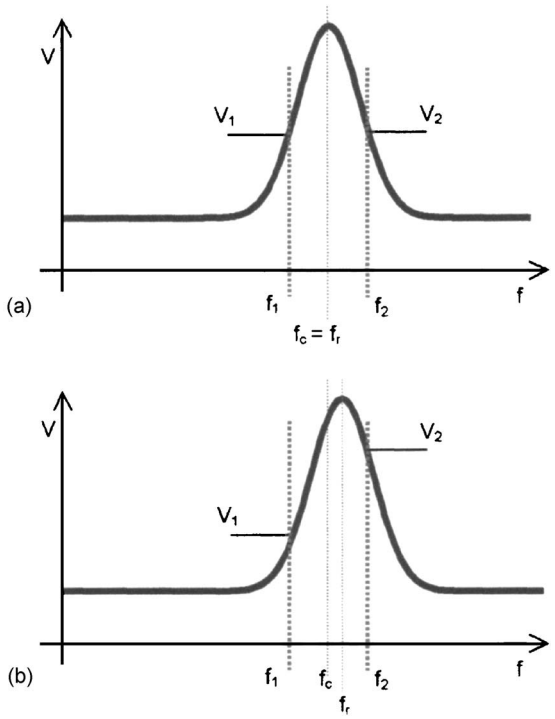

FIG. 10. Diagram of a typical output signal from the detector as a function of rf source frequency near resonance with (a) under no strain and (b) under compressive strain.

Downloaded 30 Nov 2011 to 132.170.72.241. Redistribution subject to AIP license or copyright; see http://rsi.aip.org/about/rights_and_permissions

quency response of the cavity sensor. The detection scheme operates by modulating the rf signal between two frequencies, f_1 and f_2, at a rate f_m as

$$f_1 = f_c - \Delta f, \quad f_2 = f_c + \Delta f, \tag{4}$$

where f_c is the rf center frequency. The corresponding detector response is $V_1 = V(f_1)$ and $V_2 = V(f_2)$, respectively. Note that Δf is adjustable and is not related to Δf_r, which is due to strain on the sensor. The output signal from the rf detector will comprise a component, $(V_1 + V_2)/2$, and an ac component at the frequency f_m, denoted as $v_{\text{det}} = (V_2 - V_1)/2$.

The ac component of the detector signal is a square wave form and is phase referenced to the modulating source. The amplitude is dependent on how close f_c is to f_r. Referring to Fig. 10(a), and assuming a symmetric frequency response around f_r, the ac detector signal, when $f_c = f_r$ will be

$$v_{\text{det}}\big|_{f_c=f_r} = \left[V(f_2)\big|_{f_c=f_r} - V(f_1)\big|_{f_c=f_r} \right]/2 \approx 0. \tag{5}$$

The output of the lock-in amplifier, which is referenced to f_m, will also be zero. If the resonant frequency is shifted by amount $\Delta f_r = f_r - f_c$ due to compressive strain, as shown in Fig. 10(b), then the ac detector signal, at the modulation frequency f_m, will be

$$v_{\text{det}}\big|_{f_c=f_r-\Delta f_r} = \left[V(f_2)\big|_{f_c=f_r-\Delta f_r} - V(f_1)\big|_{f_c=f_r-\Delta f_r} \right]/2. \tag{6}$$

For small changes in resonant frequency, $\Delta f_r \ll f_r/Q$, and when f_c is near f_r, the detector signal can be approximated as

$$\begin{aligned} v_{\text{det}}\Big|_{f_c=f_r-\Delta f_r} \approx & \left[\left(V(f_2)\big|_{f_c=f_r} - \Delta f_r \left.\frac{dV(f_2)}{df}\right|_{f_c=f_r} \right) \right. \\ & \left. - \left(V(f_1)\big|_{f_c=f_r} - \Delta f_r \left.\frac{dV(f_1)}{df}\right|_{f_c=f_r} \right) \right] \Big/ 2 \\ \approx & \Delta f_r \left.\frac{dV(f_1)}{df}\right|_{f_c=f_r} = \Delta f_r \frac{dV(f_r - \Delta f)}{df}, \end{aligned} \tag{7}$$

where a symmetric frequency response has been assumed. The signal is zero when $\Delta f_r = 0$, as expected.

Using Eq. (3), where the strain, ε, is related to the shift in resonant frequency as

$$\varepsilon = \frac{\Delta l}{l} \approx -\frac{\Delta f_r}{f_r}, \tag{8}$$

the detector output signal as a function of strain is

$$v_{\text{det}} = -\varepsilon f_r \frac{dV(f_r - \Delta f)}{df}. \tag{9}$$

VII. SENSITIVITY AND THEORETICAL NOISE ESTIMATE

The resolution of the measurement system will be a function of the signal amplitude and the noise level at the detector output. For the phase-sensitive detection scheme, the received signal as a function of strain is determined by Eq. (9), and is dependent on the resonant frequency and the term dV/df. The maximum signal is achieved when Δf, and thus f_1 and f_2, are chosen so that dV/df is maximized. Referring to Fig. 10, and assuming a high Q second-order resonator sensor, the optimal signal is obtained when Δf is chosen as

$$\Delta f_{\max} = \frac{f_r}{\sqrt{8}Q}; \tag{10}$$

$$\left.\frac{dV}{df}\right|_{\max} = \left.\frac{dV(f_1 = f_r - \Delta f)}{df}\right|_{\Delta f = \Delta f_{\max}} = V_{\max}\left(\frac{4Q}{3\sqrt{3}f_r}\right), \tag{11}$$

where $V_{\max} = V(f_r)$ is the maximum response from the detector. The maximum received voltage response for the sensor system shown in Fig. 8 can be estimated using

$$V_{\max} = V(f_r) = P_{\text{rf}} D_{\text{rf}} (IL_{\text{WC}})^2 G_A CF(f_r, P_{\text{rf}}). \tag{12}$$

Here P_{rf} is the transmitted power delivered to the antenna by the rf generator, D_{rf} is the on–off duty cycle of the received rf signal as controlled by the switch, G_A is the power gain of the low-noise amplifier and IL_{WC} is the path loss of the wireless rf channel between the transmit antenna and the sensor antenna. The factor CF is the rf power to voltage conversion factor for the detector.

For a typical application of our sensor system, $P_{\text{rf}} = 1$ mW, $D_{\text{rf}} = 0.1$, $\text{IL}_{\text{WC}} = 0.0032$ (−25 dB), $G_A = 890$ (29.5 dB) and CF = 350 mV/mW. This yields a maximum detector signal of $V_{\max} = 0.32$ mV. Using Eqs. (10) and (11), and for a sensor with $f_r \sim 2.5$ GHz and $Q \sim 1000$, the optimum $\Delta f_{\max} = 884$ kHz and $dV/df|_{\max} = 100$ mV/GHz. Thus, from Eq. (9), the rms detector output signal, when f_c is near f_r, will be

$$V_{\text{rms}} = 250 \text{ nV}/\mu\varepsilon. \tag{13}$$

The received signal in the interrogation system is directly dependent on the term dV/df, and thus on the quality factor of the cavity sensor. It is also strongly dependent on the wireless channel path loss, IL_{WC}, which can be improved using a more directive antenna.

The resolution of the strain measurement system will be limited by several sources of noise. Assuming that electrical noise in the receiver signal path of the interrogation system is the dominant noise source, the minimum measurable strain can be estimated using Eq. (9) as

$$\varepsilon_n = \frac{V_n}{f_r dV/df|_{\max}}. \tag{14}$$

Here V_n is the effective noise voltage at the input of the lock-in amplifier. The thermal noise, due to the video output resistance of the diode detector, would dominate the noise from the front end of the receiver system. Assuming a high-impedance load, such as the lock-in amplifier, the thermal noise voltage at the output of the detector can be estimated as

$$V_{\text{th}} = \sqrt{4kR_D TB}, \tag{15}$$

where R_D is the effective output resistance of the detector, k is Boltzmann's constant (J/K), T is the absolute temperature of the receiver (293 K at room temperature) and B is the system bandwidth (Hertz), which is determined by the lock-in amplifier settings. A typical $R_D = 100\ \Omega$ yields a

Downloaded 30 Nov 2011 to 132.170.72.241. Redistribution subject to AIP license or copyright; see http://rsi.aip.org/about/rights_and_permissions

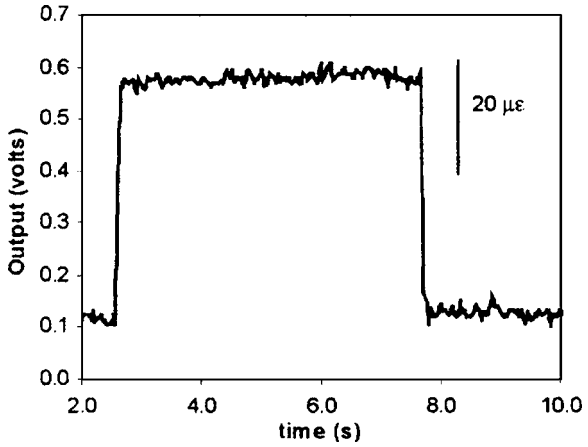

FIG. 11. Lock-in amplifier output signal for a step offset in the center frequency of 100 kHz from the resonant frequency (corresponding to 40 $\mu\varepsilon$).

thermal noise voltage of $V_{\text{th}}=1.3\ \text{nV}/\sqrt{\text{Hz}}$. However, the effective input noise of the lock-in amplifier is $7\ \text{nV}/\sqrt{\text{Hz}}$, and is the dominant noise source in our system.

For typical operation of the sensor system, and using $dV/df|_{\max}=100\ \text{mV/GHz}$ with $f_r=2.5$ GHz, the noise voltage and resulting resolution can be determined as

$$V_n = 7\ \text{nV}/\sqrt{\text{Hz}}, \quad \varepsilon_n = 28\ n\varepsilon/\sqrt{\text{Hz}}. \tag{16}$$

To measure the resolution of the system shown in Fig. 8, an offset of 100 kHz from the resonant frequency was intentionally applied at the rf source, so that $f_c=f_r$-100 kHz. This reproduces the same effective frequency shift Δf_r as if the source was fixed at the unstrained resonant frequency and the sensor device was subjected to a compressive strain of approximately 40 $\mu\varepsilon$. The output of the lock-in amplifier during this test is shown in Fig. 11, where a time constant of 10 ms was set at the lock-in amplifier (corresponding to a bandwidth B=25 Hz). The 100-kHz frequency offset produced an output of ~440 mV. This indicates a conversion ratio, due to the gain of the lock-in amplifier, of approximately $11\ \text{mV}/\mu\varepsilon$. A peak-to-peak noise of approximately 50 mV is observed in Fig. 11, with a corresponding rms noise of 10 mV. Using the same conversion ratio, this indicates a resolution of slightly less than 1 $\mu\varepsilon$. The measured noise is significantly greater than the theoretical estimate, from Eq. (16), of $\varepsilon_n\times\sqrt{B}=140\ n\varepsilon$ and implies that noise sources other than those discussed above are significant. The additional noise may be due to FM noise at the rf source and $1/f$ noise in the detector electronics. If the noise can be reduced to the thermal level of the detector, the sensitivity of this technique can be improved by a factor of 3.

The rms noise level of the system, as measured for different time constant settings, τ, on the lock-in amplifier, is shown in Fig. 12. As expected, the noise level shows a square root increase with decreasing time constant (increasing bandwidth). Also, the rms noise falls to below 10 mV for $\tau\geqslant 10$ ms, but remains fairly constant after this.

Although signal-to-noise in the present system is adequate for many purposes, it is still above the thermal noise limit. Reflected signals from the environment, which interfere with the signal returned from the sensor, have been observed. The interfering signals are greatly reduced due to the time-domain gating function of the rf switch. The reflected signals from the environment are expected to dissipate rapidly, as compared with the returned signal from the high Q sensor. The sensor is highly resonant and will continue to emit a signal well after environmental reflections have dissipated. A typical detector output signal as a function of time is shown in Fig. 13. More sophisticated gating methods can be employed to fully isolate the sensor-returned signal from the environmental reflections. These techniques have been successfully used in the past with surface acoustic wave-based sensors in order to reduce environmental reflections.[12]

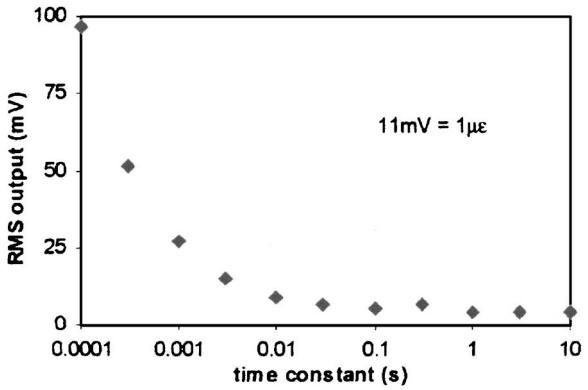

FIG. 12. Root mean square noise at the lock-in amplifier output as a function of time constant.

VIII. DISCUSSION

We have presented a type of strain sensor with application in structural health monitoring. The sensor is based on the principle of electromagnetic resonance in a cavity. The strain sensor is a passive device and requires no power to operate. Furthermore, the sensor is amenable to simple and robust construction, requires no permanent physical connection to a data acquisition unit, and can be interrogated remotely by rf signals. It is capable of unambiguous measurement of strain with high resolution. This class of embeddable sensor will have applications for damage assessment in civil structures. Resonators constructed with different materials and geometries may also have applications in other fields such as aerospace and biomedicine.

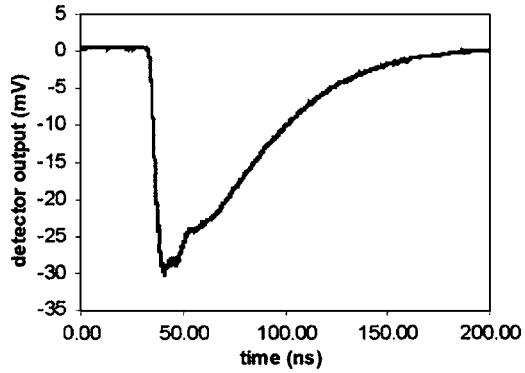

FIG. 13. Plot of a typical detector output response vs time.

Downloaded 30 Nov 2011 to 132.170.72.241. Redistribution subject to AIP license or copyright; see http://rsi.aip.org/about/rights_and_permissions

ACKNOWLEDGMENTS

The authors gratefully acknowledge the support of the Natural Sciences and Engineering Research Council of Canada (NSERC) and the National Centre of Excellence, ISIS Canada.

[1] S. C. Liu and M. Tomizuka, *Proceedings of 4th International Workshop on Structural Health Monitoring*, 2003, Stanford, CA, pp. 42–52.
[2] R. M. Measures, M. M. Ohn, S. Y. Huang, J. Bigue, and N. Y. Fan, Smart Mater. Struct. **7**, 237 (1998).
[3] D. Inaudi, S. Vurpillot, N. Casanova, and P. Kronenberg, Smart Mater. Struct. **7**, 199 (1998).
[4] R. C. Tennyson, A. A. Mufti, S. Rizkalla, G. Tadros, and B. Benmokrane, Smart Mater. Struct. **10**, 560 (2001).
[5] J. Ou, Z. Zhou, and X. Zhao, *Proceedings of 4th International Workshop on Structural Health Monitoring*, 2003, Stanford, CA, pp. 180–187.
[6] C. Doyle, C. Staveley, and P. Henderson, *Proceedings of 4th International Workshop on Structural Health Monitoring*, 2003, Stanford, CA, pp. 944–951.
[7] A. Loulizi, Ph. D. thesis, Virginia Polytechnic Institute and State University, Blacksburg, 2001.
[8] D. Pozar, *Microwave Engineering*, 2nd ed. (Wiley, New York, 1998), pp. 318–323.
[9] *Stanford Research Systems SC10 High Stability Ovenized 10 MHz Quartz Oscillator Datasheet*, http://www.srsys.com/html/sc10.html, http://www.srsys.com/html/sc10specs.html
[10] J. Chuang, M. Sc. dissertation, University of Manitoba, Winnipeg, 2004.
[11] C. A. Balanis, *Antenna Theory, Analysis and Design* (Wiley, New York, 1997).
[12] W-E. Bulst, G. Fischerauer, and L. Reindl, IEEE Trans. Ind. Electron. **48**, 265 (2001).

Downloaded 30 Nov 2011 to 132.170.72.241. Redistribution subject to AIP license or copyright; see http://rsi.aip.org/about/rights_and_permissions